Tactile Sensing over Articulated Joints with Stretchable Sensors

Tapomayukh Bhattacharjee *   Advait Jain   Sarvagya Vaish   Marc D. Killpack   Charles C. Kemp

Healthcare Robotics Lab
Georgia Institute of Technology

ABSTRACT

Biological organisms benefit from tactile sensing across the entire surfaces of their bodies. Robots may also be able to benefit from this type of sensing, but fully covering a robot with robust and capable tactile sensors entails numerous challenges. To date, most tactile sensors for robots have been used to cover rigid surfaces. In this paper, we focus on the challenge of tactile sensing across articulated joints, which requires sensing across a surface whose geometry varies over time. We first demonstrate the importance of sensing across joints by simulating a planar arm reaching in clutter and finding the frequency of contact at the joints. We then present a simple model of how much a tactile sensor would need to stretch in order to cover a 2 degree-of-freedom (DoF) wrist joint. Next, we describe and characterize a new tactile sensor made with stretchable fabrics. Finally, we present results for a stretchable sleeve with 25 tactile sensors that covers the forearm, 2 DoF wrist, and end effector of a humanoid robot. This sleeve enabled the robot to reach a target in instrumented clutter and reduce contact forces.

Index Terms: Tactile Sensing, Fabric-based Stretchable Sensors, Joint Sensing, Manipulation in Clutter

1 INTRODUCTION

Robotics researchers have demonstrated many uses for tactile sensing [5, 11]. Tactile sensors can provide useful information when in direct contact with the world. As such, having more of a robot's surface area covered with tactile sensors provides more opportunities for sensing. Within this paper, we focus on the challenge of covering articulated joints with tactile sensors. While many tactile sensors have been characterized for operation on rigid surfaces, relatively few have been shown to operate over articulated joints (see Section 2).

The geometry and exposed area of an articulated joint's surface can change over time. One potential solution is to specifically design a robot's joint so that it solely consists of rigid components covered by tactile sensors and avoids gaps. While potentially feasible, this approach restricts the design of the joints and may be unsuitable for existing robots that have not been designed with this in mind. The approach we explore in this paper is to cover the articulated joint of a robot with a flexible and stretchable sensor that can adapt to changes in the joint over time, which relates to the manner in which human skin covers articulated joints. This approach results in a number of challenges since the tactile sensing surface tends to stretch or fold during joint motion (see Fig. 1), which can have significant implications in terms of the mechanics, electrical properties, and signal processing associated with the sensor.

We first provide evidence for the value of tactile sensing over articulated joints by empirically estimating the likelihood of contact for a simple simulated arm reaching in clutter (Section 3). We then model the stretching required for a tactile sensor to cover a 2 DoF
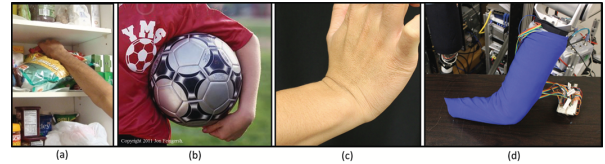
*e-mail: tapomayukh@gatech.edu

Figure 1: (a), (b)[Copyright 2011 Jon Feingersh] Many day-to-day activities involve contact with articulated joints, such as at the wrist, elbow, and fingers. (c) As articulated joints bend, human skin stretches and folds. (d) A stretchable fabric-based tactile sensing skin on a robot's wrist stretches and folds.

wrist joint (Section 4). Next, we present a flexible and stretchable fabric-based sensor that we have developed that can meet this requirement (Section 5). We then characterize our sensor with an emphasis on its performance while covering an articulated joint (Section 6). Finally, we present brief examples of our sensor being used as it covers the forearm, end effector, and 2 DoF wrist of a humanoid robot (Section 6.5.3).

2 RELATED WORK

Researchers have developed numerous tactile sensors as discussed in recent surveys [5, 7]. Despite a long history of research in this area, integration of tactile sensing over large areas of a real robot's surface is still uncommon, as is sensing over a robot's articulated joints [15].

2.1 Large-area Tactile Sensing

There have been some studies in which tactile sensors covering large surfaces of robot parts have been developed. Such tactile sensors have often used flexible printed circuit boards (PCBs) (e.g, [12, 6, 15]). These sensors are not easily adaptable to cover the joints of a robot because they do not stretch and can exhibit fatigue on repeated bending.

2.2 Stretchable and Flexible Tactile Sensors

Prior research has also used resistive and conductive fabric, rubber and other flexible, and in some cases stretchable, materials to make tactile sensors (e.g, [13, 9, 2, 16, 8]). Their physical sensing mechanisms are similar to ours, but most of these sensors have not been demonstrated on a robotic system or characterized when covering articulated joints. We first described our tactile sensor design in [10]. Our design is inspired by an open source project called rSkin [14]. [3] briefly describes contemporaneous research that has resulted in a similar fabric-based stretchable tactile sensor intended for covering compliant surfaces, such as the finger pads of a human hand. The authors characterized their sensor's change in resistance in unstretched, 5%, and 15% stretched conditions, but they have not presented results from covering articulated joints nor using their sensor with a real robot.

2.3 Tactile Sensing over Joints

While researchers have recognized that tactile sensors that stretch and bend could be valuable for covering the joints of a robot [15, 8],

few sensors have been characterized and evaluated covering the joint of a real robot. [2] present a sensor that can be used to cover the elbow of a human or humanoid robot. The sensor uses electrical inverse tomography, which has the drawback of a complex inverse problem [18, 5]. [9] used conductive thread and fabric to make a whole-body tactile sensing suit that produced binary contact signals. Quantifying the sensory input beyond a binary value is important, since it can enable the robot to regulate its contact with the world, such as by keeping contact forces low.

3 FREQUENCY OF CONTACT AT THE JOINTS

In this section, we provide evidence for the value of tactile sensing over articulated joints. In particular, we show that contact can occur frequently at the joints of a simulated robot arm as it reaches into clutter using only haptic sensing. Having tactile sensing at the joints enables the simulated robot to directly regulate contact forces at the joints.

We performed experiments with the planar simulation described in [11] in which a simulated robot arm uses model predictive control to reach into clutter. The unmodeled clutter is made of spatially uniformly distributed cylindrical fixed and movable objects and the robot arm is modeled after the three joints of a 50th percentile male including mass, link length and width [1]. We used the Open Dynamics Engine simulation [17] which simulates contact forces using linear complementarity constraints. Interested readers may refer to [11] for more details. A representative screenshot of the simulation is in Figure 2 with only movable obstacles.
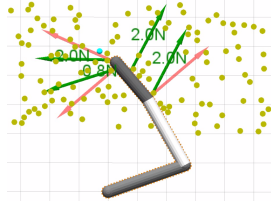

Figure 2: *Overhead view of our planar simulation of a three link robot reaching into a cluttered workspace and making contact across its entire arm. The red arrows are normal forces used in our controller and the green arrows represent the total contact force that the arm experiences. The small orange dots represent tactile sensing elements, and the yellow circles are movable cylinders.*

We ran a set of trials with varying types of objects (fixed or movable) and numbers of objects using this software simulation testbed and computed the percentage of trials in which the robot made contact with a cylindrical object at a joint at least once. Figure 3 illustrates when we considered contact to have occurred at a joint of the simulated robot. Table 1 shows the simulated arm made contact at the joints in 10.9% to 64.1% of the trials depending on the total number of cylinders and the ratio of fixed to movable objects in the clutter.
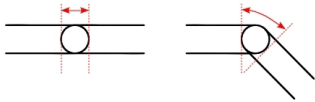

Figure 3: *For computing the results shown in Table 1, if the arm made contact with an object at a location between the dashed red lines, we considered it a contact at a joint of the robot.*

Figure 4 shows a histogram of the number of times contact occurred at locations along the length of the arm over all of the trials. It shows the robot arm fully extended on the x-axis. The

Table 1: *Percentage of trials with contact at a joint in varying levels of clutter.*

	Total number of cylinders			
	20	40	80	120
0% movable, 100% fixed	32.2%	40.0%	22.5%	10.9%
50% movable, 50% fixed	30.9%	43.4%	44.7%	39.1%
100% movable, 0% fixed	22.2%	43.1%	62.8%	64.1%

y-axis shows the number of contacts that occurred at tactile sensing elements (taxels) at the corresponding distance along the arm (x-axis), regardless of the side upon which the taxel was located. The red dotted lines designate the taxels corresponding with the robot's joints. The taxels at the front of the arm make contact most frequently, but the taxels associated with the most distal joint (the wrist) also make contact frequently.
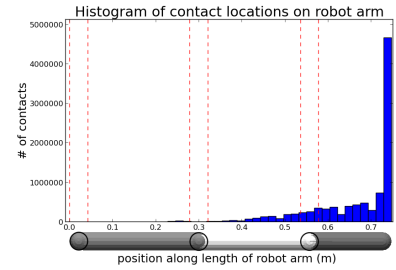

Figure 4: *Histogram of frequency of contact at different locations along the simulated robot arm. The joints are noted by the red dotted lines.*

4 A MODEL OF SENSOR STRETCH

In this section, we present a simple kinematic model that estimates the stretch required for a tactile sensor to cover a 2 DoF wrist joint (see Fig. 5). We assume that the tactile sensor covers the outer surface of the arm and its end points are rigidly fixed to the two links at a distance of L_1 and L_2 from the joint axis.
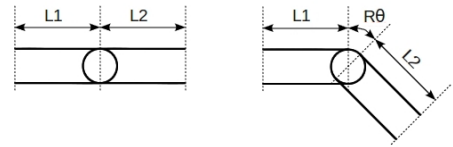

Figure 5: *Illustration of our model of stretching when a wrist bends from its neutral pose (see Eqs. 1 and 2).*

We start by considering a planar model of an arm with a 1 DoF wrist joint. We assume that there is no stretching when the distal link is collinear with the proximal link, which we refer to as the neutral pose and for which we make $\theta = 0$ (see Fig. 5). If the joint rotates to an angle $\theta \geq 0$ from its neutral pose, the length to be covered with tactile sensors increases by $R\theta$, where R is the width of the two links and the radius of the joint. So, the ratio of the new length and the unstretched length of a tactile sensor covering the arm is given by

$$s = \frac{L_1 + L_2 + R\theta}{L_1 + L_2} \quad (1)$$

$$= 1 + \beta\theta, \quad (2)$$

where s is the ratio by which the sensor stretches and β is the ratio of the radius of the arm at the joint and the unstretched length of the tactile sensor ($\beta = \frac{R}{L_1 + L_2}$). If we keep either θ or β constant, the stretch of the sensor is a linear function of the other variable. This illustrates that increasing the radius of the arm, R, increases the required stretch, and that having attachment points that are farther away from the joint can reduce the required stretch.

To extend this model to a 2 DoF wrist, we denote unit vectors along the central axes of the two links as $\hat{v}_1$ and $\hat{v}_2$, with each vector pointing towards the distal end of its link. Once again, we consider the neutral pose to occur when $\hat{v}_1$ and $\hat{v}_2$ are collinear. We model the required stretch using our 1 DoF model in Eq. 2 by assuming that the links are cylinders with radius R, the joint is a sphere with radius R, and $\theta = \arccos(\hat{v}_1 \cdot \hat{v}_2)$. This is an approximation, since it ignores possible effects of the links rotating around their central axes.

5 A STRETCHABLE TACTILE SENSOR

In this section, we present an example of a tactile sensor over an articulated joint that uses stretchable conductive and resistive fabrics.

5.1 Single Taxel

A single sensing element or taxel (short for tactile pixel) consists of five layers of fabric, illustrated in Fig. 6. The layer in the middle is resistive fabric, which is sandwiched between two layers of conductive fabric. The resistance between the two electrodes made of conductive fabric decreases given an applied force that compresses the layers.
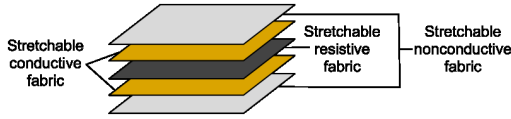

Figure 6: *Five layers of conductive, resistive and nonconductive fabric that make up our tactile sensor.*

The fabrics that we used to construct our sensor, follow:

- ***Stretchable conductive fabric:*** From Less EMF Inc., we purchased "Stretch Conductive Fabric (Cat. #321)", which is a silver-coated fabric made of 76% nylon and 24% elastic fiber.

- ***Stretchable resistive fabric:*** From Eeonyx, we purchased the EeonTex fabric named "LG-SLPA-16K" with a specified surface resistance of 16KΩ/sq. This is a a knitted nylon and spandex fabric with a proprietary conductive coating.

- ***Stretchable nonconductive fabric:*** We purchased a sleeveless compression shirt for athletes made by McDavid. The fabric is 80% nylon and 20% spandex.

5.2 Sleeve Design with an Array of Taxels

To make an array of tactile sensors, we laser cut one of the layers of conductive fabric to have multiple discrete conductive patches (electrodes) of the desired shapes and sizes. We then sew these electrodes to a layer of insulating fabric with space separating them so that they are insulated from one another (see Figure 7). By having a separate wire go to each insulated electrode, we reduce the possibility of cross-talk that can occur during multi-contact conditions with grid-based wiring, as seen with the original rSkin design [14]. We leave the remaining conductive fabric layer as a single sheet in order to serve as a common ground for all the taxels, and we place a single sheet of resistive fabric between this common ground layer and the electrode layer. As with the single taxel design, we also have an insulating layer on the exposed side of the common ground layer.

For the humanoid robot Cody, we designed a single sleeve with 25 taxels that covers the end effector, 2 DoF wrist joint, and forearm (see Figures 7 and 12). To fabricate the sensor, we laser cut the fabrics and sewed them together. Due to the presence of 25 distinct taxels operating in parallel, the sleeve can detect multiple contacts simultaneously. The output of an individual taxel depends on the resistance between the taxel's discrete electrode and the common ground layer, R_{tax}. Prior to analog to digital conversion, the only signal conditioning we perform is to put R_{tax} into a resistive voltage divider with R_{div}, where $R_{div} > 0\Omega$. The output voltage of this voltage divider is converted to a digital signal via the analog to digital converter of an Arduino Mega 2560 R3 board, which linearly converts the 0 to 5 volt analog signal to a 10-bit digital signal. We refer to a taxel's digital signal resulting from this analog to digital conversion as ADC. Since the input to the voltage divider is 5 V, $ADC = \lfloor \frac{1024}{5V} \frac{R_{tax}}{R_{tax} + R_{div}} 5V \rfloor = \lfloor \frac{1024 R_{tax}}{R_{tax} + R_{div}} \rfloor$

The ends of the sleeve are anchored to the proximal end of the forearm and the distal end of the end effector. Otherwise, the sleeve is allowed to slide across the underlying 2 DoF wrist joint and the rigid surfaces of the forearm and end effector. With respect to our model of stretch in Eq. 2, $L1 = 250.7mm$, $L2 = 200.9mm$, $R = 75.6mm$, and $\beta = 0.167$. Where $L1$ relates to the forearm length and $L2$ relates to the end effector length. Given the wrist's maximum angle from neutral, $\theta = 55°$, our model predicts that the tactile sleeve will need to stretch by 16%. Interestingly, the predicted stretch required for $\theta = 70°$, which is not achievable with Cody's wrist, would be 20%, which is very close to the 20.4% stretch estimated in [4] for human skin when a human wrist undergoes a 70° bend.
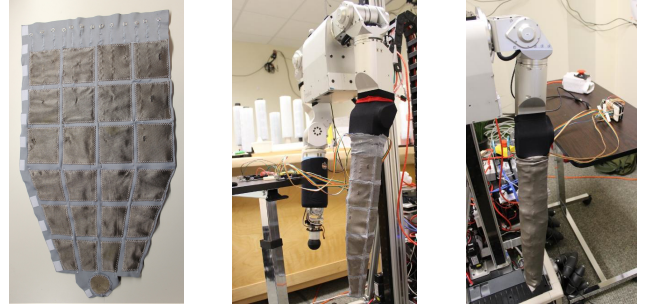

Figure 7: *Insulating fabric with 25 electrodes of conductive fabric (left) spread out, (middle) mounted on the robot, and (right) with the resistive layer and conductive layer added.*

6 SENSOR CHARACTERIZATION

In this section, we characterize the relationship between the output of the tactile sensor and the total force applied to the sensor.

6.1 Experiments : Single-Taxel Characterization

We fabricated a square tactile sensor with sides of length 5cm and pushed down on it with a tool instrumented with an ATI Nano25 (with a calibration of SI-125-3) six-axis force-torque sensor. We varied the contact region to be a square with sides of length 1cm, 2cm, and 4cm by placing squares that we cut out of acrylic on the tactile sensor before pressing with the instrumented tool. We used a fixture to guide the motion of the instrumented tool to keep the applied forces normal to the surface of the taxel. To collect data, we first set the variable ADC_{bias} so that $ADC_{bias} - ADC$ was 0 when the plastic acrylic square and the plastic tool were resting on the tactile sensor without an applied force. Next, we pushed down on the taxel

via the plastic tool and then reduced the force we applied until we were applying no force. While doing so, we logged the output of the tactile sensor and the component of the force in the vertical direction measured by the force-torque sensor. Figure 8 shows the different components of our test setup.
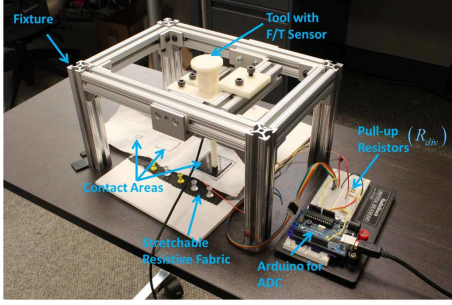

Figure 8: *Components of the test setup that we used to investigate some of the properties of the tactile sensor.*

6.2 Sensor Output and Total Force

Figure 9 shows the relationship between the normal force applied to a tactile sensor (y-axis) and $ADC_{bias} - ADC$ (x-axis) for different contact regions with $R_{div} = 200\Omega$. The hysteresis of the tactile sensor is seen in the curves associated with the increase and then the decrease of the applied force.

A more striking cause of the spread in the force for a given tactile sensor output is the variation in the contact region. A higher force distributed over a larger contact region can produce the same tactile sensor output as a lower force over a smaller contact region. As a result, there is more uncertainty about the force applied to a larger taxel, since a wider range of contact areas are possible. With a smaller taxel, a tighter bound can be placed on the maximum applied normal force that could result in an observed taxel output. Specifically, we would expect the maximum possible applied normal force to be the normal force that when uniformly distributed across the entire taxel area results in the observed tactile sensor output.

We modeled this behavior by fitting a cubic polynomial to the data from 1 cm and 2 cm taxels to obtain the coefficients of the polynomial as shown in Eq. (3). Figure 9 shows the results in which we fit the data to the 1 cm and 2 cm taxels and tested the fit to the 4 cm taxel. We cross-validated the model by switching the training and testing sets (i.e., 3 permutations). The resulting cross-validated RMS error was 8.77N.

$$y = 9.27 \times 10^{-6} \left(\sqrt{area}\right) x^3 - 8.46 \times 10^{-3} \left(\sqrt{area}\right) x^2 + 2.96 \left(\sqrt{area}\right) x + 93.45 \sqrt{area} \tag{3}$$

6.3 Effect of the Voltage-Divider Resistor

In this section, we analyze the effect of our choice of R_{div} for the voltage divider on the sensitivity of the tactile sensor. We conducted experiments with three different resistance values as shown in Fig. 10 on a contact area with side length = 4cm. Fig. 10 shows that for a given force, as the value of R_{div} increases, $ADC_{bias} - ADC$ increases. As can be seen in the figure, the highest of the three resistors better uses 10-bit digital signal.

We modeled this behavior by fitting a cubic polynomial to the data of 47 Ω and 200 Ω resistors to obtain the coefficients of the polynomial as shown in Eq. (4). Figure 10 shows the results in which we fit the data to the 47 Ω and 200 Ω resistors and tested the fit to the 470 Ω resistor. We cross-validated the model using the
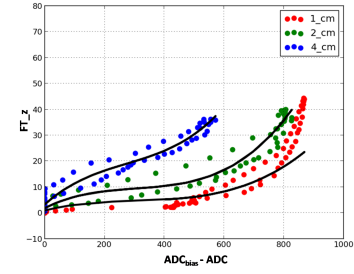

Figure 9: *Relationship between total force and tactile sensor output. The red, green and blue scatter plots correspond to square contact regions with sides of length 1cm, 2cm and 4cm respectively and the black lines show the fit.*

3 permutations of training and test data, which resulted in a cross-validated RMS error of 6.77N.

$$y = 1.64 \times 10^{-5} (R_{div})^{-3/4} x^3 - 1.348 \times 10^{-2} (R_{div})^{-3/4} x^2 + 5.51 (R_{div})^{-3/4} x + 176.93 (R_{div})^{-3/4} \tag{4}$$
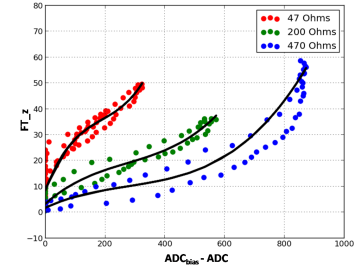

Figure 10: *The tactile sensor output varies with different values for R_{div}. For smaller values of R_{div}, the sensor is less responsive to low and moderate forces when compared to higher values of R_{div}.*

6.4 Effect of Stretching

We conducted experiments to analyze the effect of stretch on the sensor performance. We used $R_{div} = 47\Omega$ for these experiments. The unstretched length of the taxel was 25.07mm. To analyze the effect of stretch, we stretched the sensor to 40.04mm which is around 59.71% stretch. We also collected data for medium stretch of 29.85%. The results of the experiments are shown in Fig. 11.

Both the Medium and Full Stretch conditions are large relative to the 16% required stretch predicted by our model for our sleeve design. The Medium Stretch corresponds with $\theta = 102.17°$ for Cody's wrist and Full Stretch corresponds with $\theta = 204.37°$.

From Fig. 11, we see that as we stretch the sensor, both the sensitivity and hysteresis increase. We modeled the trend by fitting a cubic polynomial to the Unstretched and Medium Stretch data to obtain the coefficients of the polynomial as shown in Eq. (5), where s is the ratio by which the skin is stretched. Figure 11 shows the results in which we fit the curve to the Unstretched and Medium Stretch data and tested the fit to the Full Stretch data. We cross-validated the model using the 3 permutations of training and test data, which resulted in a cross-validated RMS error of 11.65N. The major cause of the error was hysteresis, which we did not explicitly model.

$$y = 2.16 \times 10^{-6} \left(1 - \sqrt{s}\right) x^3 - 1.23 \times 10^{-3} \left(1 - \sqrt{s}\right) x^2 + 0.299 \left(1 - \sqrt{s}\right) x + 8.65 \tag{5}$$
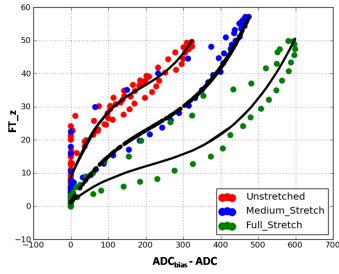
Figure 11: *Effect of stretch on the sensitivity of the stretchable sensor. Stretching the sensor increases the sensitivity and increases the hysteresis effects.*

Figure 13: *(left) The mean and standard deviation of a taxel's output without external contact as the wrist's angle changes. (right) The mean and standard deviation for the same taxel with intermittent contact as the wrist's angle changes.*

6.5 More Experiments : Tactile Sensing Sleeve

Our previous characterization was limited to testing a single taxel sitting on a flat plane. Ultimately, we are interested in the performance of our tactile sensor when actually covering the articulated joint of a real robot. For the rest of this paper, we report results from tests using the tactile sensing sleeve we developed to cover the forearm, end effector, and 2 DoF wrist of the humanoid robot Cody (see Fig. 12). For these experiments, we used a 68Ω resistors.
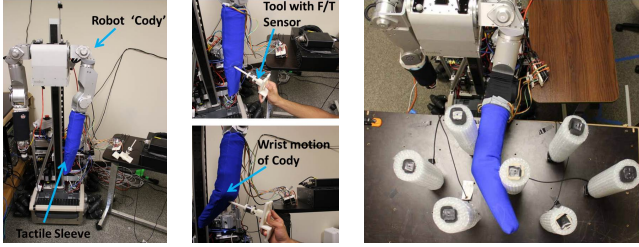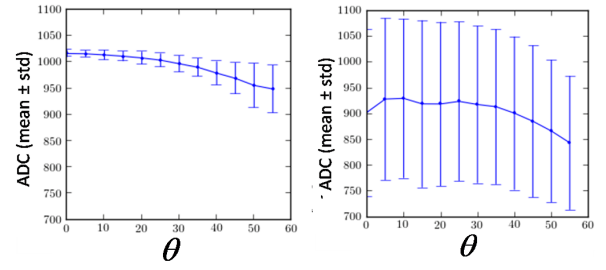

Figure 12: *(left) Cody with the tactile sensing sleeve. (middle) Experimental setup to characterize a taxel during wrist motion. (right) Cody reaching through instrumented clutter and making wrist contact.*

6.5.1 Wrist Motion without External Contact

For our first experiment, we implemented a motion that covers the workspace of the robot's wrist repeatedly with the pitch and yaw motions sweeping over their entire $45°$ to $-45°$ ranges. We collected data from a taxel on the wrist with an area of $39 cm^2$ while Cody's wrist moved in this manner for 25 minutes without external contact. Fig. 13(left) shows the mean and standard deviation of the taxel's output (ADC) as a function of θ. We see that the mean of the taxel output decreases and its standard deviation increases as the angle of the wrist increases. Consequently, large angles can result in the taxel hallucinating contact. These hallucinations are probably due to the taxel stretching, folding, and otherwise deforming at large angles. In contrast, for $\theta < 20°$ (i.e., 40 degree range of motion), the sensor readings are fairly consistent.

6.5.2 Wrist Motion with External Contact

To characterize the performance of the sensor during contact, we conducted an experiment with intermittent contact with the same taxel while the wrist made the same motion (see Figure 13(right)). An experimenter made contact with the taxel using a tool with a $39.7 mm^2$ tip instrumented with an F/T sensor that was used to obtain measurements of the force applied along the axis of the tool. During the experiment, we recorded tuples consisting of the taxel output, the measured contact force, and θ.

To evaluate the sensor's performance as θ increases, we considered detection of whether or not the taxel is in contact (see Fig. 14). With respect to this detection problem, we computed true-positive rates, false-positive rates, and F-Scores for various detection thresholds on the taxel output. For ground-truth non-contact sensor readings, we used our data from the wrist moving without external contact. For ground-truth contact sensor readings, we used a subset of our data from the wrist moving with intermittent contact. Specifically, we used the subset of data associated with one of two intervals of contact forces measured by the instrumented probe ([1N 5N] or [2N 5N]), since we would not expect a sensor to detect forces below some value and because we wanted a well-represented interval of forces. Since we operated the tool by hand, the applied forces varied widely. To analyze the performance in a way that can be better replicated, when computing the true-positive rate, false-positive rate, and F-score, we reweighted the samples in order to approximate a uniform distribution over the interval of contact forces ([1N 5N] and [2N 5N]). We also divided the data based on θ (0 to 55 degrees in 5 degree increments).

As θ increases, the false-positive rates increase. Interestingly, the true-positive rates also increase with higher stretch due to the changes in sensitivity seen in Section 6.4. *ADC* thresholds of 950 and lower have low false-positive rates up to $\theta \approx 35°$ ($\approx 70°$ range of motion). Figure 13 shows similar structure without much change in the output signal up to $\theta \approx 35°$. This is a promising result, since this evaluation treats all samples independently without the potential advantages of filtering over time or compensating for hysteresis.

6.5.3 Robot Reaching through Clutter with Tactile Sleeve

We also performed an experiment in which the objective was to have Cody autonomously reach to a goal location through an instrumented clutter field as shown in Fig. 12. We performed six trials using tactile sensing from the sleeve and another six trials using only the compliance of the arm. We found that using tactile sensing and the controller from [11], Cody successfully reached the goal location all six times. However, without using tactile sensing, Cody failed all six times. The failures were due to high forces measured from the instrumented clutter field (exceeding a safety threshold of 40N) while reaching through the clutter. The histograms of the tactile sensor readings and force readings for the reaching trials are given in Fig. 15. The figure shows that by using the tactile sensing sleeve, the controller can regulate the taxel outputs ($ADC_{bias} - ADC$) to be mostly below the specified threshold of 150. Moreover, in doing so, it was also able to keep the actual contact forces lower, even though the relationship between contact forces and taxel output is complex. *An accompanying video shows that in order to complete the task successfully, the robot-arm had to make contact with taxels at its wrist joint.*
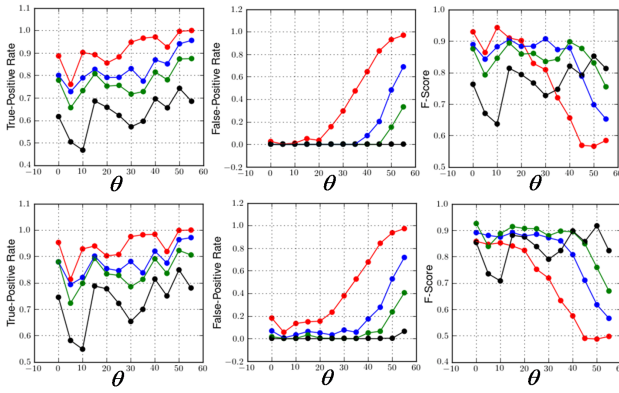
Figure 14: *(left) true-positive rates, (middle) false-positive rates, and (right) F-Scores for detecting contact with forces in the (top row) [1N 5N] and (bottom row) [2N 5N] intervals. Detection was based on the output (ADC) from a taxel on Cody's wrist. The red, blue, green, and black colors denote detection thresholds of 1000, 950, 900, and 800 respectively, where ADC higher than the threshold is labeled as "no contact".*
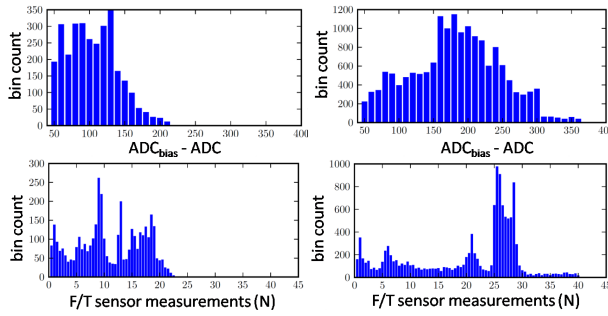

Figure 15: *Histograms from (left column) reaching with tactile sensing and (right column) reaching without tactile sensing. They show (top row) tactile sensor output and (bottom row) forces applied to the instrumented objects.*

7 CONCLUSION

In this paper, we investigated the problem of tactile sensing for articulated joints. Through a simulated robot arm reaching in clutter, we provided evidence that contact can occur frequently at a robot's joints. We then presented a simple model for the amount of stretching required for a tactile sensor to cover a 2 DoF wrist joint. We did not, however, investigate the role of compression and folding. As an example of a stretchable sensor, we described an inexpensive, robust, and easy to fabricate stretchable tactile sensor made out of stretchable fabric. We performed experiments to characterize the properties of this type of tactile sensor using a single taxel with an emphasis on characteristics relevant to covering an articulated joint. We also developed a tactile sensing sleeve with 25 taxels that covers the forearm, 2 DoF wrist, and end effector of a humanoid robot. We tested the response of a single taxel on this sleeve at the wrist while the robot changed the configuration of its wrist. Although the sensor has hysteresis and relatively large taxels, our evidence suggests that the sleeve can be useful for contact detection over an angular range of approximately 70°. We also demonstrated that the sleeve can be used to enable a robot to reach into clutter and reduce contact forces. More generally, we expect that our approach and methods could be useful for the development of future tactile sensors for articulated joints.

REFERENCES

[1] Man-Systems Integration Standards - Anthropometry and Biomechanics, 1995.

[2] H. Alirezaei, A. Nagakubo, and Y. Kuniyoshi. A tactile distribution sensor which enables stable measurement under high and dynamic stretch. In *3D User Interfaces, 2009. 3DUI 2009. IEEE Symposium on*, pages 87–93. IEEE, 2009.

[3] G. Büscher, R. Kõiva, C. Schürmann, R. Haschke, and H. J. Ritter. Flexible and stretchable fabric-based tactile sensor. In *IEEE/RSJ International Conference on Intelligent Robots and Systems (IROS 2012), Workshop on Advances in Tactile Sensing and Touch based Human-Robot Interaction*, Vilamoura, Algarve, Portugal, Oct. 2012.

[4] F. Cody, R. Idress, D. Spilioti, and E. Poliakoff. Tactile spatial acuity is reduced by skin stretch at the human wrist. *Neuroscience Letters*, 484:71–75, 2010.

[5] M. R. Cutkosky, R. D. Howe, and W. R. Provancher. *Force and Tactile Sensing*, chapter 19. Springer Handbook of Robotics, 2008.

[6] M. R. Cutkosky and J. V. Ulmen. Dynamic Tactile Sensing. In V. Santos and R. Balasubramanian, editors, *The Human Hand: A Source of Inspiration for Robotic Hands*, chapter 24. Springer Berlin Heidelberg, 2012.

[7] R. Dahiya, G. Metta, M. Valle, and G. Sandini. Tactile sensingfrom humans to humanoids. *IEEE Transactions on Robotics*, 26(1):1–20, 2010.

[8] T. Hoshi and H. Shinoda. A sensitive skin based on touch-area-evaluating tactile elements. In *Haptic Interfaces for Virtual Environment and Teleoperator Systems, 2006 14th Symposium on*, pages 89–94. IEEE, 2006.

[9] M. Inaba, Y. Hoshino, K. Nagasaka, T. Ninomiya, S. Kagami, and H. Inoue. A full-body tactile sensor suit using electrically conductive fabric and strings. In *Intelligent Robots and Systems' 96, IROS 96, Proceedings of the 1996 IEEE/RSJ International Conference on*, volume 2, pages 450–457. IEEE, 1996.

[10] A. Jain. *Mobile Manipulation in Unstructured Environments with Haptic Sensing and Compliant Joints, Chapter-4*. PhD thesis, Georgia Institute of Technology, July 20, 2012.

[11] A. Jain, M. D. Killpack, A. Edsinger, and C. C. Kemp. Reaching in clutter with whole-arm tactile sensing. *to appear in the International Journal of Robotics Research (IJRR)*, 2013.

[12] O. Kerpa, K. Weiss, and H. Worn. Development of a flexible tactile sensor system for a humanoid robot. In *Intelligent Robots and Systems, 2003.(IROS 2003). Proceedings. 2003 IEEE/RSJ International Conference on*, volume 1, pages 1–6. IEEE, 2003.

[13] T. Papakostas, J. Lima, and M. Lowe. A large area force sensor for smart skin applications. In *Sensors, 2002. Proceedings of IEEE*, volume 2, pages 1620–1624. IEEE, 2002.

[14] H. Perner-Wilson and I. Danforth. rSkin – Open Source Robot Skin, http://www.instructables.com/id/rSkin-Open-Source-Robot-Skin/.

[15] A. Schmitz, P. Maiolino, M. Maggiali, L. Natale, G. Cannata, and G. Metta. Methods and technologies for the implementation of large-scale robot tactile sensors. *IEEE Transactions on Robotics*, (99):1–12, 2011.

[16] M. Shimojo, A. Namiki, M. Ishikawa, R. Makino, and K. Mabuchi. A tactile sensor sheet using pressure conductive rubber with electrical-wires stitched method. *Sensors Journal, IEEE*, 4(5):589–596, 2004.

[17] R. Smith et al. Open dynamics engine http://www.ode.org, 2011.

[18] D. Tawil, D. Rye, and M. Velonaki. Improved eit drive patterns for a robotics sensitive skin. In *Proceeding of Australasian Conference on Robotics and Automation (ACRA)*, pages 2–4, 2009.